Electronics and Electrical Engineering

http://www.aimspress.com/journal/ElectronEng

AIMS Electronics and Electrical Engineering, 6(1): 29–42.
DOI: 10.3934/electreng.2022003
Received: 26 November 2021
Accepted: 11 January 2022
Published: 14 January 2022

Research article

Millimetre wave 3-D channel modelling for next generation 5G networks

Latih Saba'neh[1,2,*] **and Obada Al-Khatib**[2]

[1] Cisco Systems Netherlands Holding BV-KHBP, Haarlerbergweg 13, Amsterdam Zuidoost,1101CH, Amsterdam

[2] Faculty of Engineering and Information Sciences, University of Wollongong in Dubai, Dubai Knowledge Village, Dubai, 20183, UAE

* **Correspondence:** Email: lsabaneh@cisco.com.

Abstract: Millimetre wave (mm-wave) spectrum (30-300GHz) is a key enabling technology in the advent of 5G. However, an accurate model for the mm-wave channel is yet to be developed as the existing 4G-LTE channel models (frequency below 6 GHz) exhibit different propagation attributes. In this paper, a spatial statistical channel model (SSCM) is considered that estimates the characteristics of the channel in the 28, 60, and 73 GHz bands. The SSCM is used to mathematically approximate the propagation path loss in different environments, namely, Urban-Macro, Urban-Micro, and Rural-Macro, under Line-of-Sight (LOS) and Non-Line-of-Sight (NLOS) conditions. The New York University (NYU) channel simulator is utilised to evaluate the channel model under various conditions including atmospheric effects, distance, and frequency. Moreover, a MIMO system has been evaluated under mm-wave propagation. The main results show that the 60 GHz band has the highest attenuation compared to the 28 and 73 GHz bands. The results also show that increasing the number of antennas is proportional to the condition number and the rank of the MIMO channel matrix.

Keywords: 5G networks; channel modeling; millimetre wave; MIMO; wireless communications

1. Introduction

It is predicted that by the year 2021 the amount of monthly traffic generated by smart phones will hit the boundaries of 50 petabytes (i.e., 50000 terabytes) [1]. In addition, the evolving technologies, such as internet of things (IoT), virtual reality (VR), autonomous vehicles, and ultra-high transmission media (4K,8K), etc., are driving high bandwidth demands. Thus, internet service providers (ISPs) are facing global bandwidth scarcity with enormous amount of traffic and services exploiting bandwidth-hungry applications with requirements of higher data rates and lower latencies. The millimetre wave (mm-wave) spectrum (30 to 300 GHz) is a key candidate in enabling the deployment of the next 5G

cellular communication systems, which is capable of addressing the aforementioned challenges [2]. From the amount of bandwidth obtainable from the mm-wave spectrum, it will support data rates of multiple gigabits/second (Gbps) and latencies in the order of milliseconds (ms).

However, the currently accessible channel models of the 4G-LTE systems with frequencies below 6 GHz lack the capability to comprehend the characteristics of the mm-wave propagation channel, which utilises extremely high frequency (EHF) bands. This is due to the fact that, at such high frequency bands, comportment of the particles is dominant over the wave propagation comportment. Therefore, atmospheric attenuation caused by particles interaction with radio waves becomes more significant at high frequency bands. Moreover, the main difficulty facing the operation of mm-wave is its high path loss induced by severe signal attenuation factors, such as blockage, atmospheric attenuation and foliage (e.g. trees). This will impose the necessity of deploying high gain antennas and the utilisation of multiple-input-multiple-output (MIMO) systems to compensate for the path loss [3]. Therefore, an accurate model for the mm-wave propagation channel is required to study those effects and extract the channel parameters [2].

Extensive research has been ongoing under the objective of developing a channel model that accurately convey the characteristics of the mm-wave propagation channel. When considering mm-wave spectrum, different channel features, such as atmospheric effects, line-of-sight/non-line-of-sight (LOS/NLOS) environments, and foliage loss should be interpreted. In [4], feasibility study conducted on the 28 GHz band has considered foliage loss and omnidirectional path loss in NLOS environment. However, a scarcity of atmospheric loss and LOS study weakens the proposed model. Similarly, the authors in [3] have discussed mm-wave channel propagation in NLOS environment only and discarded the effects of foliage and atmospheric loss. In addition, the research showed a lack in modelling the shadow fading effects. Some research, such as [5], has offered an additional channel modeling parameters, such as outage, in order to yield a better modelling accuracy. However, this only increases the complexity of the channel model and is similar to the outage probability in the 3GPP suburban NLOS model [6]. In [7], it has been shown that the 3GPP model, which uses the alpha-beta-gamma (ABG) path loss model, is more complex and less accurate than the close-in reference model, when implemented for the mm-wave channel characterisation. Recently, studies in various papers, such as in [8], have proposed models that evaluate mm-wave propagation in LOS environments only, discarding NLOS condition which is more critical. This is because the probability of being in a NLOS is higher, particularly when examining dense urban areas.

In this paper, an analysis and simulation framework is delivered to evaluate the performance of the mm-wave propagation channel. First, the spatial statistical channel model (SSCM) is considered to estimate the received power in LOS and NLOS environments as a function of the carrier frequency in several environmental configurations, including Urban-Macro, Urban-Micro, and Rural-Macro. Second, atmospheric effects, such as rain and humidity, have been analysed to assess their impact on the received power under several carrier frequencies. In addition, foliage loss is investigated to study the attenuation induced by it. Finally, an adequate exploitation of MIMO systems in various antenna and channel settings is studied to reflect the feasibility of mm-wave operation in MIMO systems.

The organisation of this paper is as follows. Section 2 describes the channel model, including the path loss in LOS and NLOS environments. In Section 3, the results for the evaluation and validation of the proposed analysis are provided and discussed. Finally, useful remarks close the paper in Section 4.

2. Channel model

This section provides the foreground of the mm-wave channel modelling approach. This includes an elaboration on the spatial statistical channel model (SSCM) and the mathematical formulation that embodies it. In addition, it highlights important aspects of the path loss modelling.

2.1. Path loss model

The mm-wave channel model presented in this paper is based on the 3-D spatial statistical channel model (SSCM) that uses mathematical representation to characterise the real-world channel model. The path loss model is a fundamental and a vital component for evaluating the performance of the channel. The proposed model is considered for LOS path loss and NLOS path loss, both of which are crucial in determining the power attenuation in a large-scale environment as a function of the carrier frequency and the distance between the transmitter (Tx) and the receiver (Rx). There are multiple path loss models that have been used such as the floating intercept (FI) model used by 3GPP and the ABG model in [7]. However, the path loss model considered in this paper is the close-in reference model (CI) that is simpler and more accurate than the FI and ABG model for the mm-wave channel modeling [7]. The CI reference path loss model is given by [9]:

$$PL^{CI}(f,d)[dB] = FSPL(f,1m)[dB] + 10n\log_{10}(d) + AT[dB] + X_{\sigma} \tag{2.1}$$

where $d \geq$ 1m, is the 3-D distance between the Tx and Rx in meters. $FSPL$ is an acronym for free space path loss as a function of the carrier frequency f and the 1m close-in reference distance between the Tx and the Rx. n represents the path loss exponent (PLE), AT is a term that captures the attenuation caused by the haze/fog and humidity, and X_{σ} is a Gaussian random variable with a mean of zero and a standard deviation of σ dB representing the shadowing factor in the wireless channel. As discussed in [7], the close-in reference distance is chosen to be 1m only because the base stations (BSs) in the 5G wireless networks are closer to the users than the highly-mounted enhanced-node base stations (eNBs) in 4G wireless networks, since more BSs will be located indoors for 5G. The $FSPL$ and AT are described by the following two equations respectively:

$$FSPL(f,1m)[dB] = 20\log_{10}\left(\frac{4\pi f \times 10^9}{c}\right) = 32.4[dB] + 20\log_{10}(f) \tag{2.2}$$

$$AT[dB] = \alpha[dB/m] \times d[m] \tag{2.3}$$

where α is the attenuation factor in the (1-100) GHz range. In (2.2), c denotes the speed of light in m/s, f is frequency in GHz. Note that the CI model has a frequency dependant component within the free space path loss equation.

2.2. LOS and NLOS path loss

The two environment regimes, LOS and NLOS, are key factors in characterising the path loss model. In LOS, the transmitter and the receiver are mounted in a forthright manner. On the other hand, in NLOS condition, obstacles and scatterers form a barrier between the transmitter and the receiver.

Obstructions include but are not limited to, foliage (e.g. trees) and buildings. Both conditions are essential to estimate the actual received power, which is given by [10]:

$$P_{received}(d)[dB] = P_{transmitted}[dB] - PL(d)[dB] \tag{2.4}$$

Note that the path loss PL is found by using (2.1). Therefore, the LOS and NLOS path loss can be modelled by using the close-in reference path loss model in various environment configurations as detailed below [11].

1. LOS environment
   - Urban-macro (UMa) LOS scenario:

$$PL^{CI}_{L,UMa}(f,d) = 32.4 + 20\log_{10}(d) + 20\log_{10}(f) \tag{2.5}$$

   - Urban-micro (UMi) LOS street canyon (SC) scenario:

$$PL^{CI}_{L,UMi}(f,d) = 32.4 + 21\log_{10}(d) + 20\log_{10}(f) \tag{2.6}$$

   - Rural-macro (RMa) LOS scenario:

$$PL^{CI}_{L,RMa}(f,d) = 32.4 + 21.6\log_{10}(d) + 20\log_{10}(f) + \chi_{\sigma LOS} \tag{2.7}$$

2. NLOS environment
   - Urban-macro (UMa) NLOS scenario:

$$PL^{CI}_{N,UMa}(f,d) = 32.4 + 30\log_{10}(d) + 20\log_{10}(f) \tag{2.8}$$

   - Urban-micro (UMi) LOS street canyon (SC) scenario:

$$PL^{CI}_{N,UMi}(f,d) = 32.4 + 32\log_{10}(d) + 20\log_{10}(f) \tag{2.9}$$

   - Rural-macro (RMa) LOS scenario:

$$PL^{CI}_{N,RMa}(f,d) = 32.4 + 27.5\log_{10}(d) + 20\log_{10}(f) + \chi_{\sigma NLOS} \tag{2.10}$$

The χ_σ parameter is the shadow fading such that $\chi_{\sigma LOS} = 1.7$ dB and $\chi_{\sigma NLOS} = 6.7$ dB. In (2.5)-(2.10), $d \geq 1$ represents the 3-D distance in meters between the transmitter and f is the carrier frequency in GHz [11]. The main difference between UMa and UMi scenarios is the height of the transmitter. Specifically, in UMa, the transmitter is mounted at a higher point from surrounding buildings. On the other hand, in UMi, the transmitter is mounted below the buildings nearby.

3. Results and discussion

The NYU-WIRELESS academic research center performed many mm-wave measurements for 5 years (from 2012-2017) and developed the NYUSIM software based on their findings [12]. The software offers channel impulse responses (CIR) in temporal and spatial regimes with reliable rendering (generating graphical plots from a model). In contrast with the 3GPP channel model for

frequencies below 6 GHz, the NYUSIM statistical spatial channel model (SSCM) approach provides a more accurate number of time clusters compared to that given in the 3GPP. The number of clusters considered in the 3GPP channel model was unrealistically large (12 and 19 in LOS and NLOS, respectively) and incompatible with a real-world scenario. On the other hand, the NYUSIM accounts for a realistic number of clusters (i.e. 1 to 6), which have been obtained from real world measurements conducted by field researchers.

It is noteworthy that the simulator is based on Monte-Carlo simulations in order to generate definite amount of CIRs samples at particular distance between the transmitter and receiver. The simulator allows the user to input 28 parameters, that consists of 16 channel parameters and 12 antenna parameters. Figure 1 is a screenshot of the NYUSIM software showing the default values used for the channel and antenna parameters.

In this analysis, various conditions are evaluated and assessed, such as path loss (in dB) and LOS and NLOS received power (in dBm). This is examined in certain settings relative to the channel propagation characteristics, such as LOS and NLOS conditions, UMi and UMa, different frequency bands, etc. In each configuration, 100 simulation runs are performed and the average of each value required is calculated. This is to yield an accurate result, given that the simulations use Monte Carlo

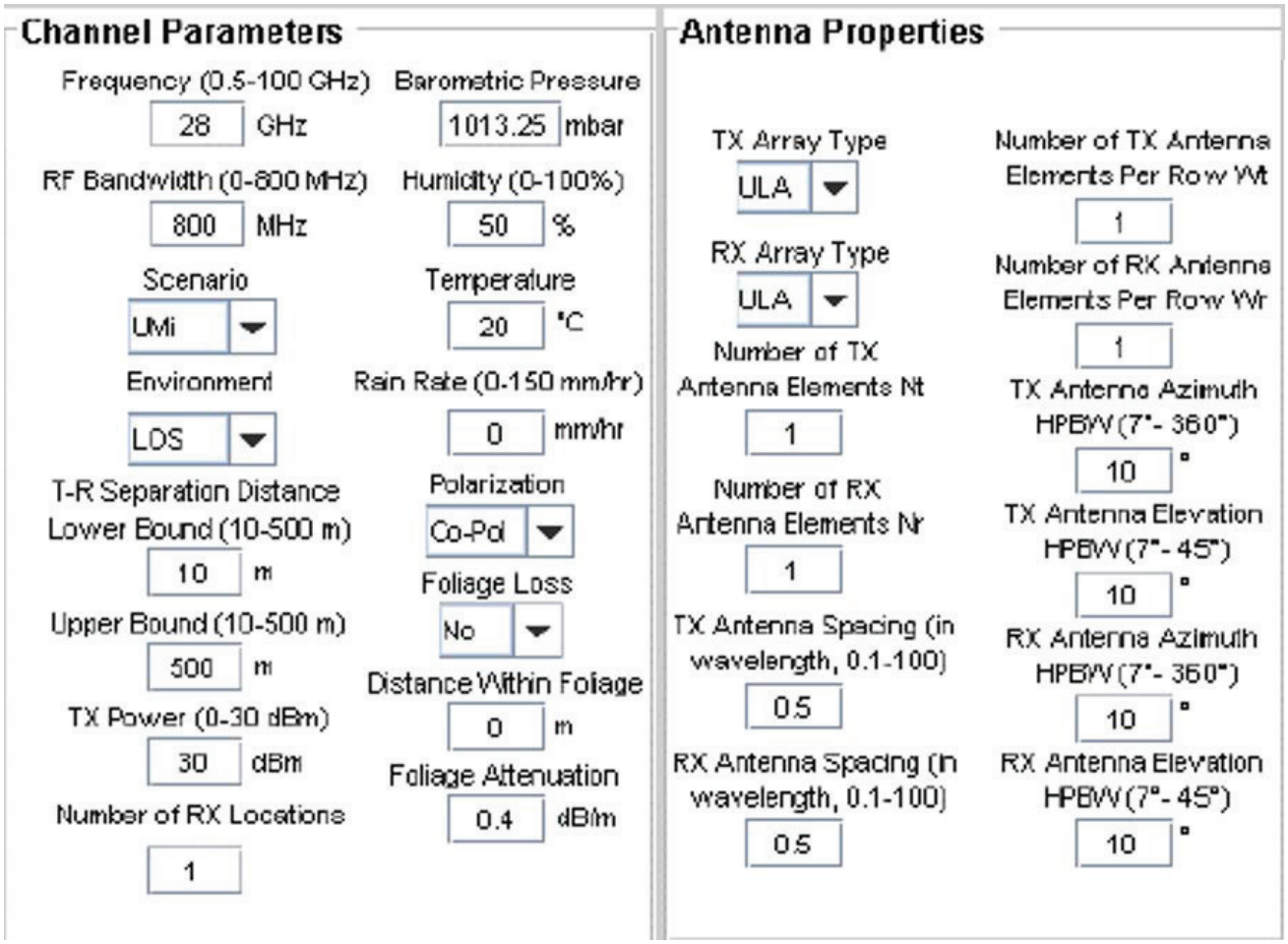

Figure 1. Default values for the channel and antenna parameters in the NYUSIM software.

simulation approach. Note that, in dBm measurements, the signal power has a range between 0 and -100 dBm and the closer the power is to 0, the stronger it is.

3.1. Received power in LOS/NLOS

This simulation focuses on the received power relative to several frequency bands over a fixed distance between the transmitter and the receiver of 200 meters. For this simulation, all parameters are kept at their default values except for the following parameters:

- Temperature: From 20 to 25 degrees Celsius
- Distance within foliage: From 0 to 1.5 meters
- Foliage loss: From No to Yes
- Upper/Lower Bound: 200 meters
- Environment: LOS/NLOS interchangeably

The frequency range is from 28 to 78 GHz and are performed for LOS and NLOS conditions to compare the received power at each regime as shown in Figure 2.

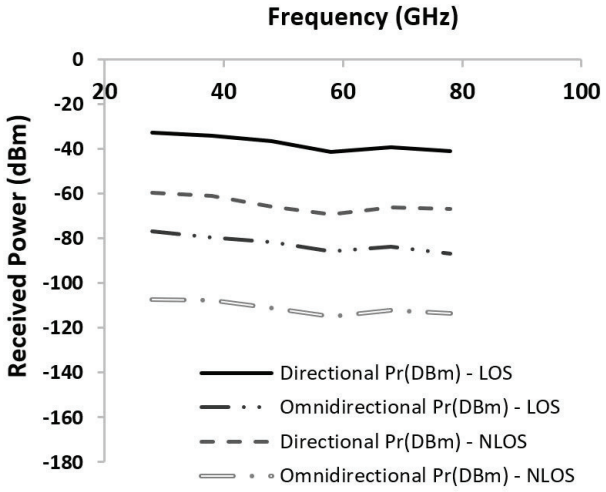

Figure 2. Received power vs. frequency in LOS and NLOS environements.

Here, the values in LOS vs those in NLOS are expected, since NLOS condition induces more attenuation due to blockage effects. Note also the difference between the results considering directional and omnidirectional propagation, where it is clear that the power dissipated in all directions is supposed to exhibit less power as opposed to directional propagation power. Furthermore, the results show a slight steep as frequency increases, where the peak is at 58 GHz. This is because the 60 GHz frequency band has a unique property that is caused by oxygen absorption that results in a surplus of attenuation as explained in [13]. However, all frequencies shown here generate a tolerable attenuation, taking into account the use of MIMO and beamforming techniques (which were not considered in this simulation).

3.2. Path loss in UMi, UMa, and RMa

This simulation examines the relation between distance and path loss in three different scenarios (i.e. UMi, UMa and RMa). For this simulation, all parameters are kept at their default values, except for the following parameters:

- Environment: NLOS
- Temperature: From 20 to 25 degrees Celsius
- Foliage Loss: From No to Yes
- Distance within foliage: From 0 to 1.5 meters

In this simulation, the transmitter-receiver distance range is 100 to 200 with a 10 meters surplus in each iteration. The frequency was kept at 28 GHz. The result is plotted in Figure 3, which shows a correlation between UMi and UMa scenarios in terms of path loss. Between 100 and 200 meters, an additional loss of merely 10 dB occurred. It can also be noted that there is a difference of 11 dB between the RMa path loss and UMi/UMa, which is also expected as rural areas are less dense than urbans areas. The rural area offers a wider coverage and a good PLE as explained and presented by [14].

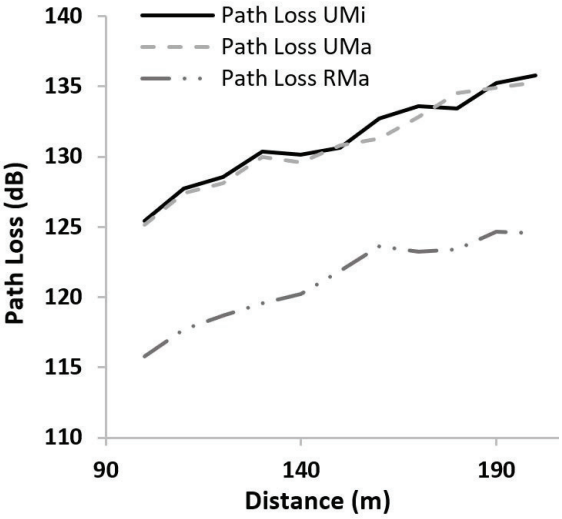

Figure 3. Path loss vs. distance.

3.3. Atmospheric conditions

First, we analyse the effect of the rain rate (mm/h) on the omnidirectional received power (dBm) of the mm-wave channel. For this simulation, all parameters are kept at their default values as shown in Figure 1, except for the following parameters:

- Temperature: From 20 to 25 degrees Celsius
- Frequency: 28, 73 and 60 GHz
- Distance Within Foliage: From 0 to 200 meters
- Distance Lower/Upper Bound: from 10 and 500 respectively to 200 meters

Figure 4 shows the omnidirectional received power as a function of the rain rate. In addition, Figure 5 shows the omnidirectional received power as a function of the humidity; however, for this simulation, the temperature is set to 20 degrees Celsius and no foliage loss is considered.

Note that the power received is in dBm (i.e., the closer the power received is to 0, the stronger it is). As shown in Figure 4, the rain rate was measured for six points from 2.5 to 10 mm/h with a

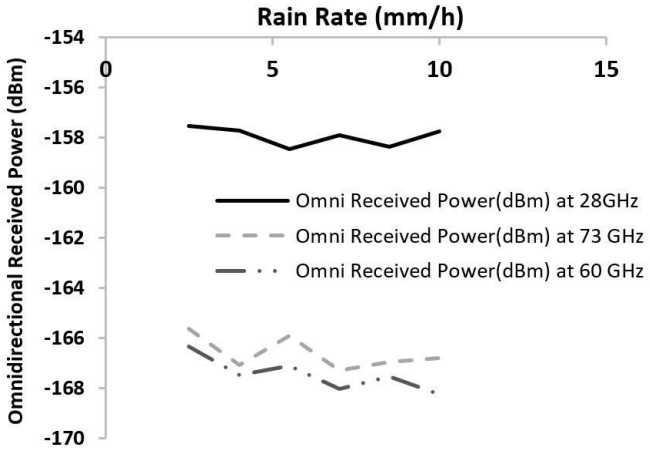

Figure 4. Omnidirectional received power vs. rain rate.

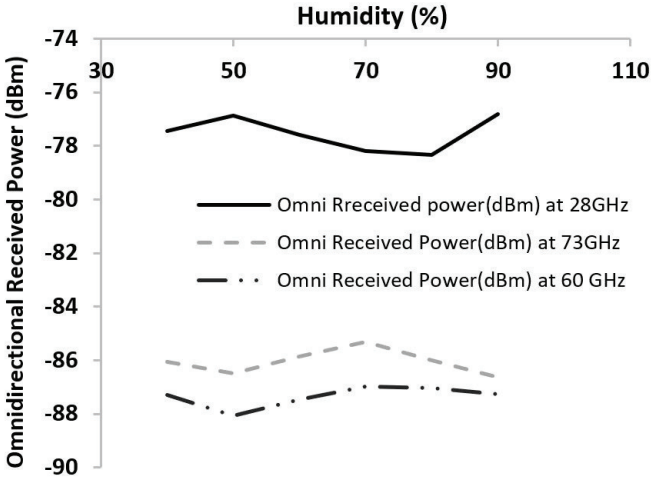

Figure 5. Omnidirectional received power vs. humidity.

1.5 alteration for each iteration. This is the typical range of a moderate rain fall. On the other hand, humidity in Figure 5 ranged from 40% to 90% (with 10% surplus in each iteration) as the typical range of humidity in multiple weather conditions. As explained by [9], in comparison with ultra-high frequency (UHF) microwave spectrum, the atmospheric loss in the mm-wave bands is merely a few extra decibels. However, an exclusion can be made to some frequency bands, such as 60 GHz. The 60 GHz band creates much higher losses and impairments to the propagated signal with distance. This significant attenuation, estimated to be 20 dB/Km [15], is caused by the atmospheric absorption, particularly by the Oxygen molecules, making the 60 GHz band suitable for short-range communications [16]. It is clear from Figure 4 that the attenuation induced by the 60 GHz band is the most significant as opposed to the other two bands. It is noteworthy that, at rain rates of 4 and 7 mm/h, the received power decreases for 60 and 73 GHz. However, the observation is different at 10 mm/h, where at 73 GHz band we have a higher received power in contrast with the 60 GHz band. Furthermore, at 28 GHz the best power received is seen at 2.5 and 10 mm/h, and the least received is at 5.5 and 8.5 mm/h. Nevertheless, the difference in power received in each band is merely a few decibels. Figure 5 clearly shows that 60 GHz records the least received power (i.e., more attenuation).

Another observation is that the effect of humidity is different at higher frequency bands as compared to lower bands. For instance, in Figure 5, two peaks can be detected at 50 and 70 percentage, where the latter offers a higher received power. However, at lower frequency bands (i.e. 28 GHz), it can be seen that, at 50 humidity percentage, a higher received power is yielded as compared to 80 percent. Thus, it can be deduced that at 70 percent humidity, high frequency bands yield a better power reception. However, at lower frequency bands, 50 percent humidity yield a better power reception. Nevertheless, it can be seen that the rain rate has a higher impact compared to humidity at higher frequency bands and vice versa.

3.4. Antenna configuration

In Figure 6, an examination of the antenna parameters is given, particularly, angles of azimuth and elevation at both the transmitter and the receiver. The main objective is to correlate the received power and the angle configuration. At the receiver, the azimuth and elevation angles are increased from 60 and 7 to 240 and 28 at step sizes of 60 and 7, respectively. For example, 60/7 antenna configuration at the receiver means that the azimuth angle is 60, while the elevation angle is 7. For the transmitter, on the other hand, we have assumed the same angle for both azimuth and elevation angles. Specifically, they are both initiated at 10 degrees up to 40 degrees, with a step size of 10 degrees. As seen in Figure 6, we have 3 high peaks happened when both the elevation and azimuth angles at the transmitter are 20 degrees under the following 3 antenna configurations at the receiver, 120/14, 180/21 and 240/28. However, at 60/7 antenna configuration at the receiver, high peak is located at an angle of 30 degrees for both elevation and azimuth angles at the transmitter, and low peak has happened at 20 degrees. Though there is no significant improvement in the received power, it can be shown that the finest power achieved is at an antenna configuration at the reciter of 120/14 and at an angle of 20 at the transmitter for both angles.

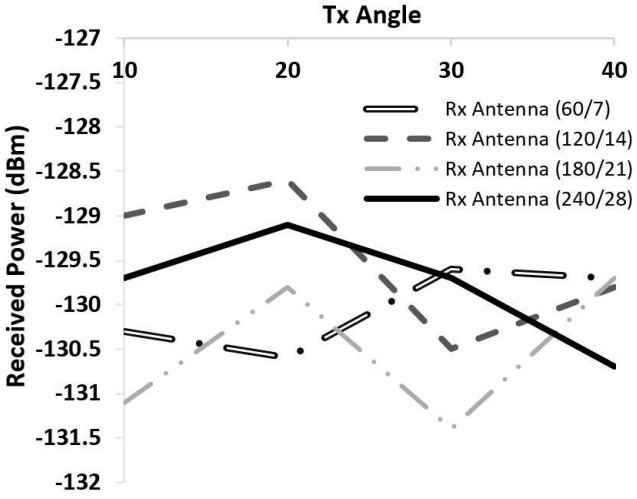

Figure 6. Received power vs. Tx angle in azimuth/elevation at 28 GHz.

In Figure 7, antenna spacing was manipulated to investigate its effect on the received power. Also, the polarization relation between the transmitter and the receiver was tested with respect to the antenna spacing and the carrier frequency, i.e., Co-Polarization (Co-Pol) and Cross Polarization (X-Pol). From

Figure 7, it is clearly shown that the received power is constant regardless of the antenna spacing, and a very slight change in the received power can be seen at an antenna spacing of 1 wavelength under the Co-Pol configuration. However, this slight change is very small and can be neglected. Thus, as far as the simulations yield, antenna spacing causes little or no improvement on the received power of the propagation signal under the same polarization configuration. However, for the same carrier frequency, we can see that Co-Pol achieves a higher received power compared to X-Pol. Moreover, for the same type of polarization, a higher power is received for the 28 GHz carrier frequency compared to the 60 GHz carrier frequency.

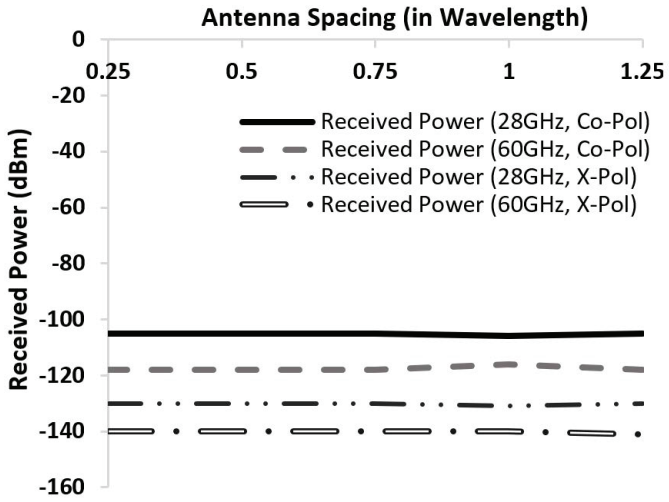

Figure 7. Antenna spacing vs. received power.

3.5. MIMO utilisation

In this simulation, we analyse different configurations of MIMO antenna elements that is supposed to improve the performance of the mm-wave channel using spatial multiplexing. An analysis of the condition number of the MIMO channel matrix $\boldsymbol{H}_w$ is performed to evaluate the efficiency of the channel. The condition number is defined as the ratio of the largest to smallest singular values in the process of breaking down the singular values of the MIMO channel matrix [12]. Furthermore, the rank of the MIMO channel matrix is also considered, which determines the number of spatial streams that can be sent at once (i.e., multiplexing) over the propagation channel. Note that this simulation assumes orthogonal frequency division multiplexing (OFDM) modulation scheme with 1600 sub-carriers. The simulation is performed at 28 and 60 GHz bands for 2×2, 3×3, 4×4 and 8×8 MIMO settings. The following is the changed parameters while all other parameters are kept at their default values:

- Temperature: 30 degrees Celsius
- Environment: NLOS
- Rain Rate: 2.5 mm/h
- Foliage Loss: Yes
- Distance within foliage: 10 meters
- Upper/Lower bound distance: 200 meters

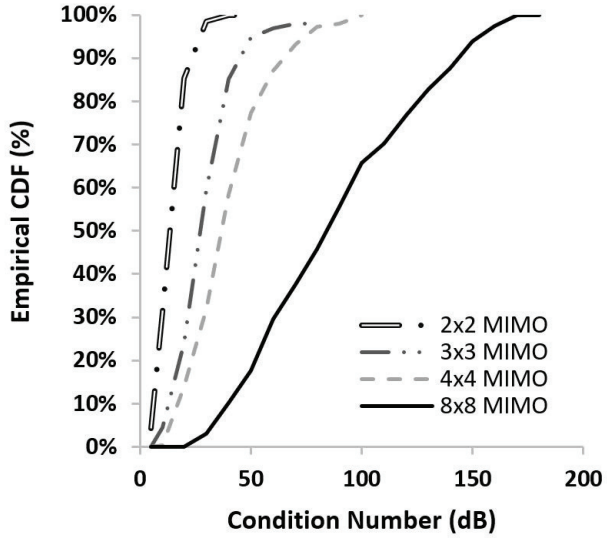

Figure 8. Empirical CDF of the condition number at 28 GHz.

Figures 8 and 9 show the empirical cumulative distribution functions (CDFs) of the MIMO condition number at 28 and 60 GHz, respectively. Note that an increase in the number of antenna elements yields an increase in the condition number. It is apparent from Figure 8 that a 3×3 MIMO has a condition number that is 30 dB larger compared to a 2×2 at 28GHz. However, from Figure 9, a difference of 20 dB is evident between the same two MIMO configurations at 60 GHz, where the condition number of a 2×2 matrix increased by 10 dB at 60 GHz compared to 28 GHz. Recall that, theoretically, a lower condition number indicates a better quality of the MIMO channel [17]. However, the reason of the high condition number of the larger MIMO channels is that the matrix becomes rank deficient. In other words, the matrix does not have a full rank.

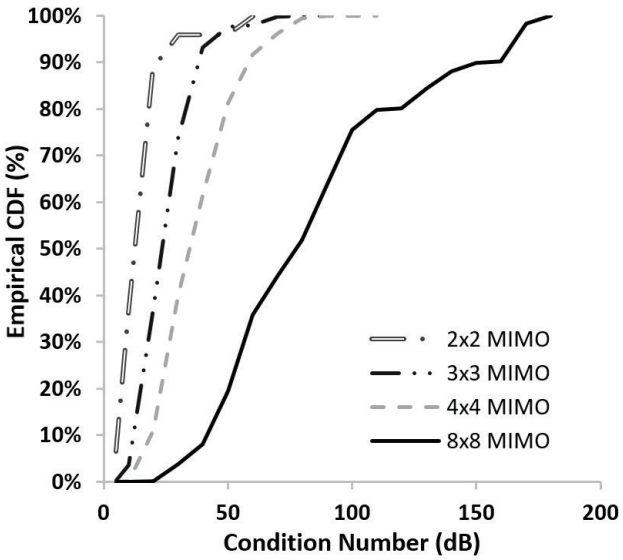

Figure 9. Empirical CDF of the condition number at 60 GHz.

Figures 10 and 11 correspond to the rank of the MIMO channel matrix at 28 and 60 GHz,

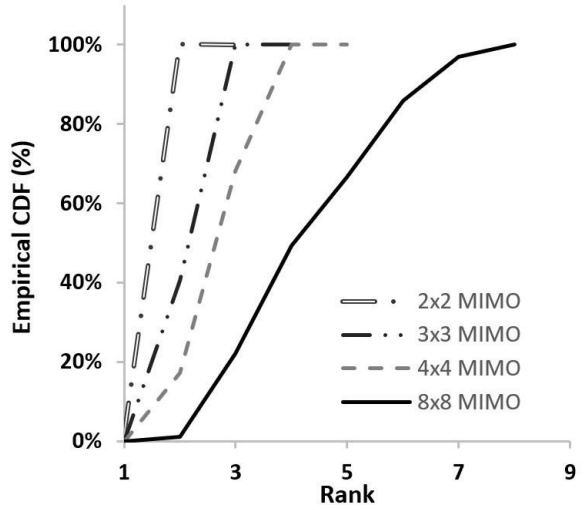

Figure 10. Empirical CDF of the channel matrix rank at 28 GHz.

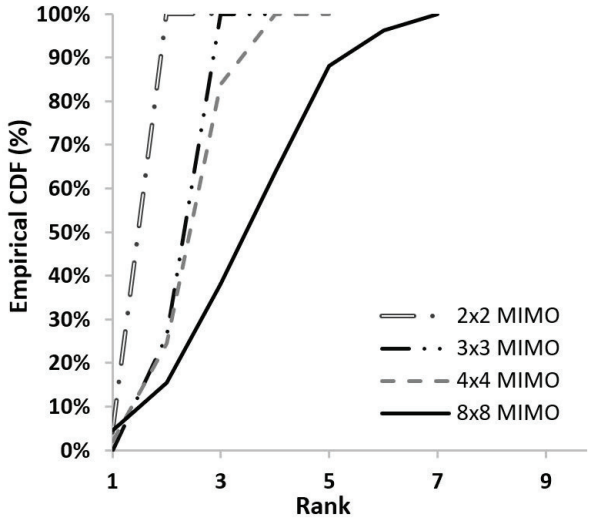

Figure 11. Empirical CDF of the channel matrix rank at 60 GHz.

respectively. Recall that the rank of the matrix indicates the number of spatial streams that can be sent at once over the channel. In this case, an 8×8 MIMO is considered the most efficient with the capability of multiplexing 8 streams over the channel at once, which is considered ideal. However, only for a small percentage of the channel matrices, a rank 8 is achieved. For instance, note that in Figures 10, 8×8 MIMO has a rank of 8 only for about 2% of the channel matrices (recall that the matrix is rank deficient). However, for the higher frequency of 60 GHz as shown in Figure 11, a rank of 7 is achieved for merely 3% of the channel matrices. Thus, we can conclude that, at higher frequencies, the capability of multiplexing decreases. Nevertheless, the behavior of MIMO at high frequency bands is still not clear and needs to be further investigation.

4. Conclusion

In this paper, an adequate channel characterisation has been made to evaluate the performance of the mm-wave propagation. various mm-wave frequency bands at LOS and NLOS were studied, where the 60 GHz band created the highest attenuation. Moreover, the received power as a function of the distance was evaluated in various scenarios, such as UMi and UMa. The effect of humidity and rain on the propagation of the mm-wave channel at different frequency bands was also investigated. For instance, specific humidity percentages showed a better received power compared to other percentiles. Finally, utilisation of MIMO was examined in terms of the condition number (dB) and the rank for different channel settings, i.e., 2×2, 3×3, 4×4 and 8×8. It was evident that the number of antenna elements is directly proportional to the condition number and the rank of the channel matrix, where an 8×8 MIMO yielded the highest multiplexing capability with a rank of 8 at 28GHz, which is ideal. In conclusion, the millimetre wave exhibits a viable propagation channel despite the attenuation factors that are caused by different environmental settings, which can be mitigated by the exploitation of MIMO spatial multiplexing. Nevertheless, future work is still desirable which includes further research on channel modelling of human blockage, studying MIMO beamforming techniques, and antenna modelling.

Conflict of interest

The authors declare that there is no interest in this paper.

References

1. Hur S, Baek S, Kim B, et al. (2016) Proposal on Millimeter-Wave Channel Modeling for 5G Cellular System. *IEEE J-STSP* 10: 454–469. https://doi.org/10.1109/jstsp.2016.2527364.
2. Xiao M, Mumtaz S, Huang Y, et al. (2017) Millimeter Wave Communications for Future Mobile Networks (Guest Editorial), Part I. *IEEE J Sel Area Comm* 35: 1425–1431. https://doi.org/10.1109/jsac.2017.2698698.
3. Li Q, Shirani-Mehr H, Balercia T, et al. (2015) Millimeter wave channel model and system design considerations. In *2015 IEEE International Conference on Communication Workshop (ICCW)*, 1214–1219. https://doi.org/10.1109/iccw.2015.7247343.
4. Ko J, Lee K, Cho YJ, et al. (2016) Feasibility study and SPATIAL–TEMPORAL Characteristics analysis for 28 GHz outdoor wireless channel modelling. *IET Commun* 10: 2352–2362. https://doi.org/10.1049/iet-com.2015.0318
5. Akdeniz M, Liu Y, Samimi M, et al. (2014) Millimeter Wave Channel Modeling and Cellular Capacity Evaluation. *IEEE J Sel Area Comm* 32: 1164–1179. https://doi.org/10.1109/jsac.2014.2328154.
6. Sun S, Rappaport TS, Rangan S, et al. (2016) Propagation path Loss models for 5G Urban micro- And Macro-Cellular Scenarios. In *2016 IEEE 83rd Vehicular Technology Conference (VTC Spring)*, 1–6. https://doi.org/10.1109/vtcspring.2016.7504435.

7. Rappaport T, MacCartney G, Samimi M, et al. (2015) Wideband Millimeter-Wave Propagation Measurements and Channel Models for Future Wireless Communication System Design. *IEEE T Commun* 63: 3029–3056. https://doi.org/10.1109/tcomm.2015.2434384.
8. Sulyman A, Nassar A, Samimi M, et al. (2014) Radio propagation path loss models for 5G cellular networks in the 28 GHZ and 38 GHZ millimeter-wave bands. *IEEE Commun Mag* 52: 78–86. https://doi.org/10.1109/mcom.2014.6894456.
9. Sun S, Rappaport T, Thomas T, et al. (2016) Investigation of Prediction Accuracy, Sensitivity, and Parameter Stability of Large-Scale Propagation Path Loss Models for 5G Wireless Communications. *IEEE T Veh Technol* 65: 2843–2860. https://doi.org/10.1109/tvt.2016.2543139.
10. MacCartney GR, Sun S, Rappaport T, et al. (2016) Millimeter wave wireless communications: new results for rural connectivity. *Proceedings of the 5th Workshop on All Things Cellular: Operations, Applications and Challenges*.
11. Marcus MJ (1994) Spectrum management implications of millimeter Wave technology. In *1994 IEEE MTT-S International Microwave Symposium Digest (Cat. No.94CH3389-4)*, 631–634. https://doi.org/10.1109/mwsym.1994.335502.
12. Kestwal M, Joshi S, Garia L (2014) Prediction of Rain Attenuation and Impact of Rain in Wave Propagation at Microwave Frequency for Tropical Region (Uttarakhand, India). *International Journal Of Microwave Science And Technology* 2014: 1-6. https://doi.org/10.1155/2014/958498.
13. International Telecommunication Union (ITU) (2005) Specific attenuation model for rain for use in prediction methods. P.838-3 (03/2005).
14. Samimi M, Rappaport T (2016) 3-D Millimeter-Wave Statistical Channel Model for 5G Wireless System Design. *IEEE T Microw Theory* 64: 2207–2225. https://doi.org/10.1109/tmtt.2016.2574851.
15. Sun S, MacCartney GR, Rappaport TS (2017) A novel millimeter-wave Channel simulator and applications for 5G wireless communications. In *2017 IEEE International Conference on Communications (ICC)*, 1–7. https://doi.org/10.1109/icc.2017.7996792.
16. NYUSIM Version 1.4 - NYU WIRELESS. NYU WIRELESS (2021) Retrieved 30 July 2021. Available from: `http://wireless.engineering.nyu.edu/nyusim-version-1-4-now-available/`.
17. Caetano L, Li S (2005) Benefits of 60 GHz: Right Frequency, Right Time. Retrieved 15 July 2021. Available from: `https://www.yumpu.com/en/document/read/27278508/benefits-of-60-ghz-energie-technik`.

AIMS Press